Available online at www.sciencedirect.com

SciVerse ScienceDirect

Ceramics International 39 (2013) 6787–6793

CERAMICS INTERNATIONAL

www.elsevier.com/locate/ceramint

Dielectric relaxation behavior and energy storage properties in $Ba_{0.4}Sr_{0.6}Zr_{0.15}Ti_{0.85}O_3$ ceramics with glass additives

Ting Wu[a,b,*], Yongping Pu[a], Kai Chen[a]

[a]School of Materials Science and Engineering, Shaanxi University of Science & Technology, Xi'an 710021, People's Republic of China
[b]Key Laboratory of Auxiliary Chemistry & Technology for Chemical Industry, Ministry of Education, Xi'an 710021, People's Republic of China

Received 23 November 2012; received in revised form 25 January 2013; accepted 6 February 2013
Available online 13 February 2013

Abstract

$Ba_{0.4}Sr_{0.6}Zr_{0.15}Ti_{0.85}O_3$ ceramics with $SrO–B_2O_3–SiO_2$ glass additives were prepared via the solid state reaction route. The effects of glass contents on the sintering behavior, dielectric properties, microstructures, and energy storage properties of BSZT ceramics were investigated. Dielectric breakdown strength of 22.4 kV/mm was achieved for BSZT ceramics with 20 wt% glass addition. Dielectric relaxation behavior was observed in dielectric loss versus temperature plots. In order to investigate the mechanism of dielectric breakdown performance, the relationship between dielectric breakdown strength and grain boundary barrier was studied by the measurements of breakdown strength and activation energy. A discharged energy density of 0.45 J/cm^3 with an energy efficiency of 88.2% was achieved for BSZT ceramics with 5 wt% glass addition.

Keywords: A. Sintering; B. Grain boundaries; C. Dielectric properties; D. Glass

1. Introduction

Future technological advances in power inversion systems based on SiC modules will depend on advances in dielectric materials with high energy and power densities. One way to achieve these advances is to develop new materials for ceramic capacitor with high energy storage density [1–3]. High energy storage density capacitors with decreased volume, weight and cost are urgently needed for electric vehicles. In accordance with the energy storage density equation for nonlinear dielectrics [4,5], two key materials parameters to obtain high energy density are high dielectric constant and high breakdown strength (BDS, E_b), while high E_b makes a more pronounced contribution toward the energy density.

Recently, $Ba_xSr_{1-x}TiO_3$ (BST) ceramics have received interest in energy storage densities of the dielectric materials because of their extremely high dielectric constants [6,7]. Unfortunately, BST ceramics have a relatively low E_b due to the existence of defects (such as pores). Researches [8–11] have shown that the substitution of Ti^{4+} with Zr^{4+} ions in BST can reduce the dielectric loss or leakage current in the material, which improved the dielectric BDS obviously. In addition, it was reported that the addition of glasses to BST ceramics notably improved its BDS as well [12–14]. However, researchers mainly focused on the effect of glass additives on the sintering temperature and microstructure, rarely mentioned on the mechanism of breakdown. Huang et al. [15] found that dielectric breakdown strength strongly depends on the interface polarization in BST glass ceramics. In fact, interface polarization is also present in the glass added ceramics. The glass located at the grain boundary or surrounding the grains in glass added ceramics [12–14], impeding the transfer of free charge, and resulting in accumulation of charges or ions in intergranular area.

In this paper, $SrO–B_2O_3–SiO_2$ glass used as sintering additives for $Ba_{0.4}Sr_{0.6}Zr_{0.15}Ti_{0.85}O_3$ (BSZT) ceramics was prepared. The effect of glass contents on the dielectric properties, microstructures, and energy storage properties

*Corresponding author at: Shaanxi University of Science and Technology, School of Materials Science and Engineering, Xi'an 710021, People's Republic of China. Tel.: +86 291 5091322819; fax: +86 290 2986168131.
E-mail address: 420501558@qq.com (T. Wu).

0272-8842/$ - see front matter © 2013 Elsevier Ltd and Techna Group S.r.l. All rights reserved.
http://dx.doi.org/10.1016/j.ceramint.2013.02.009

was investigated. In addition, we mainly discussed the dielectric relaxation behavior and the mechanism of breakdown of BSZT ceramics. The goal is to get new information on the dielectric relaxation behavior and mechanism of dielectric BDS of BSZT ceramics.

2. Experimental procedure

BSZT powder was prepared by the solid-state method using analytical reagent grade $BaCO_3$, $SrCO_3$, ZrO_2 and TiO_2 powders. Stoichiometrically weighed powders were wet-milled with distilled water for 4 h, dried and calcined at 1300 °C/4 h. According to the glass formation region [16], a glass with the composition of 51.62% SrO, 41.35% B_2O_3, 7.03% SiO_2 (weight fraction) was prepared from the analytical reagent grade carbonates or oxides. The appropriate constituents were well mixed and melted in corundum crucible at 1250 °C for 1 h. The molten glass was quenched in distilled water and then ball milled to fine powders. The glass powders were mixed with BSZT powder in the ratio corresponding to the following chemical composition: $(100-x)\%$ BSZT$+x\%$ glass (weight fraction), where $x=0$, 5, 10, 15 and 20. The mixed powders were pressed into pellets and then sintered at different temperatures for 2 h in air.

The sintered samples for dielectric measurement were polished to 0.5 mm in thickness and painted with silver paste and fired at 650 °C for 20 min. The frequency dependence of dielectric properties was measured using a precision LCR Meter (E4980A, Agilent Tech., CA, US) over a frequency range from 20 Hz to 2 MHz at room temperature, the temperature dependence of dielectric properties were measured over a temperature range from 40 to 450 °C, and the impedance data were measured over frequencies from 20 Hz to 2 MHz in a temperature range of 200–500 °C without bias voltage. The DC BDS measurement was performed using a withstanding voltage tester at room temperature. All samples were immersed in silicone oil to prevent surface flashover. At least 10 specimens were used for each composition during BDS testing. The polarization–electric field (P–E) hysteresis loops were measured using a ferroelectric tester (TF Analyzer 2000, aixACCT, Aachen, Germany) at room temperature.

3. Results and discussion

In order to determine the suitable sintering temperature (SST) [8], the bulk density of all samples sintered at different temperatures was measured by the Archimedes method. The measured density shows that the SSTs of the ceramics are 1450, 1240, 1220, 1180, and 1160 °C, when $x=0$, 5, 10, 15, and 20, respectively. The addition of glass largely decreases the SSTs of BSZT ceramics. In the rest of this paper, all the samples were prepared at their SSTs.

Fig. 1 presents the frequency dependence of dielectric constant and dielectric loss for BSZT ceramics with different glass contents. The dielectric constant of samples shows good frequency stability in the measured frequency range. Pure BSZT ceramic possesses a dielectric constant of about 1000, while the dielectric constant of BSZT ceramic with 20 wt% glass addition is only about 100, an order of magnitude reduction in dielectric constant was observed. The sharp decrease in the dielectric constant can be attributed to the addition of low dielectric constant component (glass). The dielectric loss of samples decreases gradually with increasing frequency, which tends to be stabilized at about 1×10^{-3} from 1 kHz to 2 MHz. According to the previous report [17], the dielectric loss at frequency range from 20 Hz to 1 kHz may induced by the leakage currents.

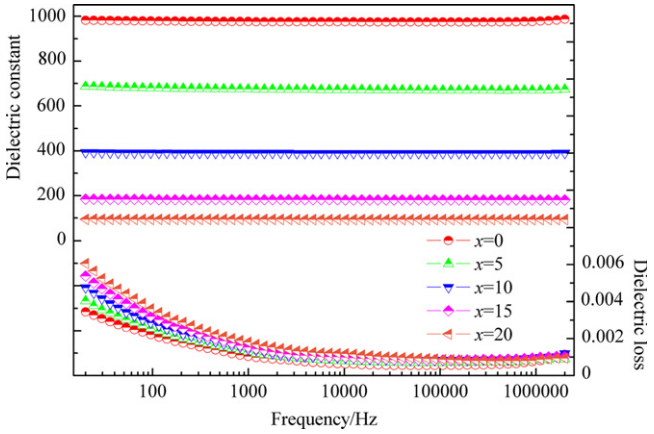

Fig. 1. Frequency dependence of dielectric constant and dielectric loss for BSZT ceramics with different glass contents.

Fig. 2 shows the variation of dielectric constant and dielectric loss with temperature at a few selected frequencies for pure BSZT ceramics and ceramics with 10 wt% glass addition. The dielectric constant and dielectric loss remain constant up to a certain temperature and thereafter, increase rapidly with increasing temperature. The temperature dependence of dielectric loss plot shows a peak. The position of the peak shifts to higher temperature with increasing frequency. Similar results were observed in other samples ($x=5$, 15, and 20). It is indicated that some relaxation polarization mechanism is existed in both pure BSZT ceramics and glass-added ceramics [18,19].

The complex impedance spectrum has been proved to be a powerful method for investigating the relaxation polarization mechanism of grain and grain boundary in ceramics [15,20]. The samples are measured at different temperatures at every 20 °C interval in order to get series of the Cole–Cole images. The complex impedance spectra measured at different temperatures for pure BSZT ceramics and ceramics with 10 wt% glass addition were presented in Fig. 3. Similar results were observed in other samples ($x=5$, 15, and 20). Two semicircles can be observed in the two diagrams, which indicate that two distinct dielectric relaxation processes exist in the sample. At low temperature (<380 °C), the first semicircle at low frequency cannot be obtained because of the high resistivity.

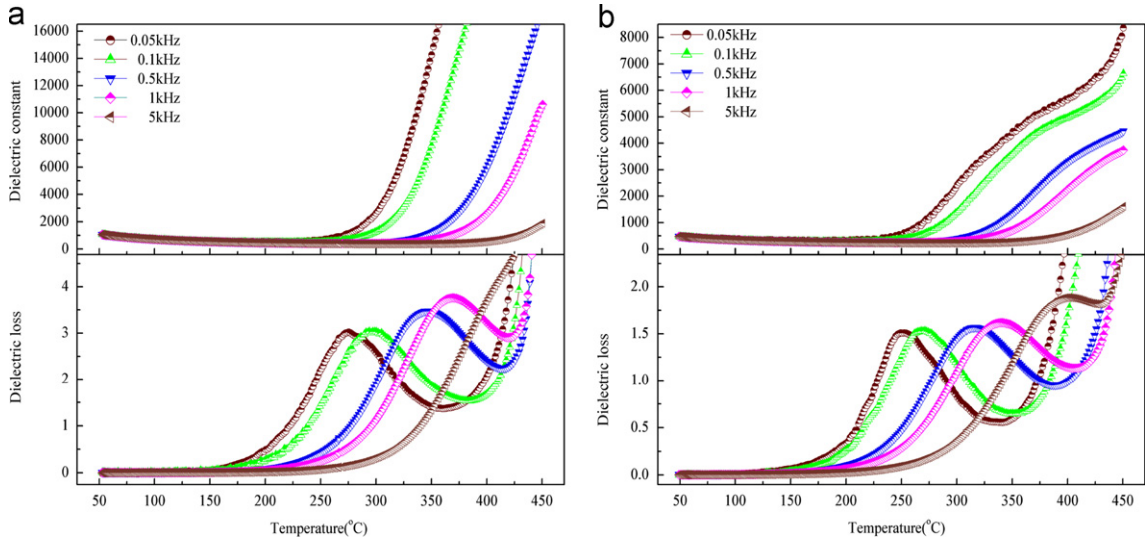

Fig. 2. Variation of dielectric constant and dielectric loss with temperature at different frequencies for pure BSZT ceramics (a) and ceramics with 10 wt% glass addition (b).

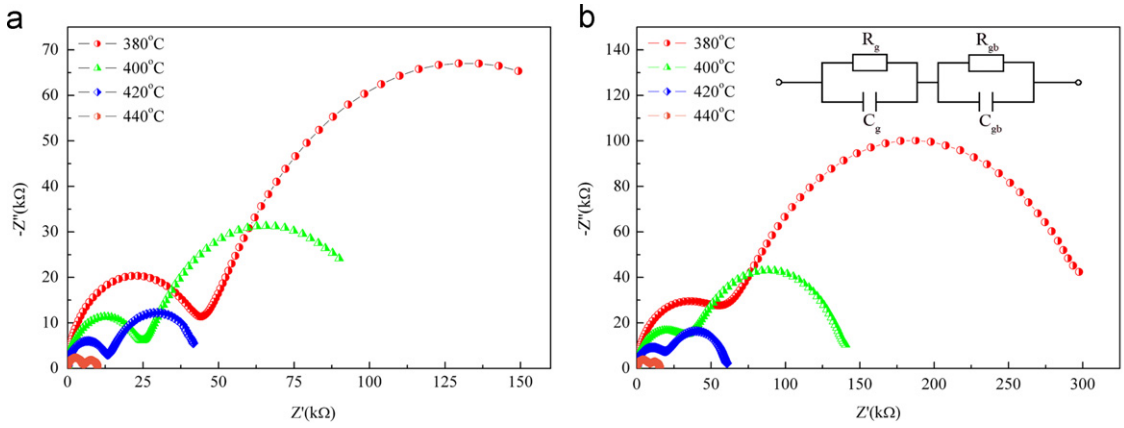

Fig. 3. Complex impedance spectra measured at different temperatures for pure BSZT ceramics (a) and ceramics with 10 wt% glass addition (b).

In general, the sample is composed of two parts, ceramic and electrode. The silver paste used in this work achieved the ohmic contact between silver electrodes and ceramic, thus the contact capacitance C_e and contact resistance R_e can be omitted. In order to model the electrical response and extract resistance and capacitance of each electroactive element, an equivalent circuit, shown in the inset of Fig. 3(b), was fitted using ZSimpwin Electrochemical Impedance Spectroscopy Data Analysis software (version 3.10). While the ceramic typically consists of grains and grain boundaries two different regions. Therefore, the two R–C circuit elements represent the contributions from the grain phases and grain boundary phases, respectively. In addition, as can be seen in Fig. 3(a) and (b), both the two impedance semicircles become smaller with increasing measuring temperature, thus the two observed dielectric relaxation behaviors corresponding to the grain boundary phases and the grain phases are correlated with the thermally activated motions of defect and polar nanoregions, respectively. Meanwhile, the impedance semicircle of grain boundary phases in Fig. 3(b) (ceramics with 10 wt% glass-added) increases obviously when compared with the impedance semicircle of grain boundary phases in Fig. 3(a) (pure BSZT ceramics). It is suggested that the effect of grain boundary phases on the ceramics is enhanced with glass addition.

The reciprocal value of measurement frequency at the extreme point of each semicircle represents the relaxation time τ at a certain measurement temperature. According to the Arrhenius relationship, the activation energy for relaxation can be calculated from the slope using the following equation:

$$\ln \tau = \frac{1}{k_B T} E_a + \ln \tau_0 \quad (1)$$

where τ_0 is a pre-exponential factor, E_a is the activation energy for the relaxation process, k_B is the Boltzmann constant and T is the absolute temperature. Fig. 4 plots the relaxation time as a function of measuring temperature for BSZT ceramic with 10 wt% glass addition, the activation

energy corresponding to the grain boundary phases ($E_{a,1}$) and the grain phases ($E_{a,2}$) can be obtained from the slope of solid lines which linear fits through the data. In our measurement condition, $E_{a,1}$ corresponds to the relaxation of space charge, which characterizes the effective energy barrier that impedes the transfer of free charge. $E_{a,2}$ corresponds to the relaxation of polar nanoregions, which characterizes the traps energy that prevents the polar nanoregions to make an orientation under external electric field.

The microstructures of pure BSZT and glass-added specimens were observed in Fig. 5. Two effects of glass addition on the microstructure could be observed. On one hand, the grain size reduced notably and distributed more uniform. As shown in Fig. 5(a), pure BSZT has large grains and uneven distribution, while the grain size of BSZT with glass-added decreases and the distribution is more uniform (Fig. 5(b), (c) and (d)). On the other hand, further addition of the glass led to unobvious grain boundary (Fig. 5(e)).

Fig. 6 shows the Weibull distribution of the BDS for BSZT ceramics with different glass contents. This distribution has been found, both in theory and in practice, to be most appropriate for the BDS analysis. The reasonable values of BDS can be calculated by the Weibull linear equation which is described in detail elsewhere [3,15]. As can be seen in Fig. 6, all the five samples fit well with the Weibull distribution, and an increasing the Weibull modulus m was observed with increase in glass content, thus the samples have a more concentrative distribution of BDS as well.

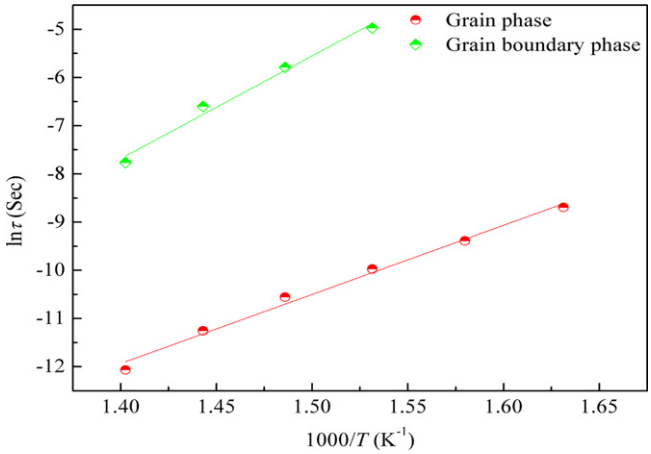

Fig. 4. Relaxation time as a function of $1000/T$ for BSZT ceramic with 10 wt% glass addition. The solid lines are linear fits through the data.

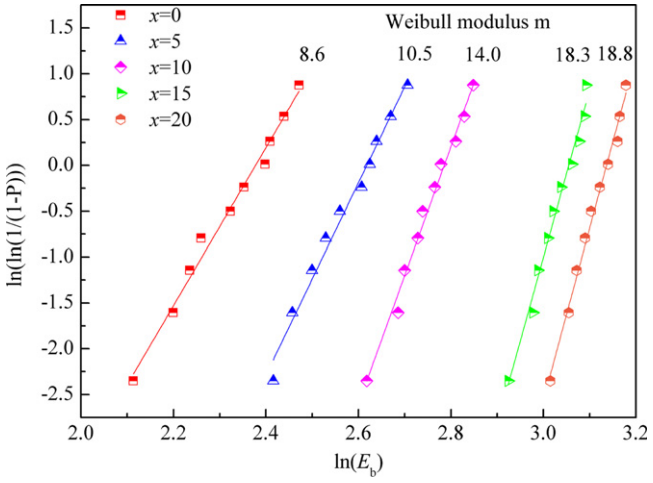

Fig. 6. Weibull distribution of the BDS for BSZT ceramics with different glass contents.

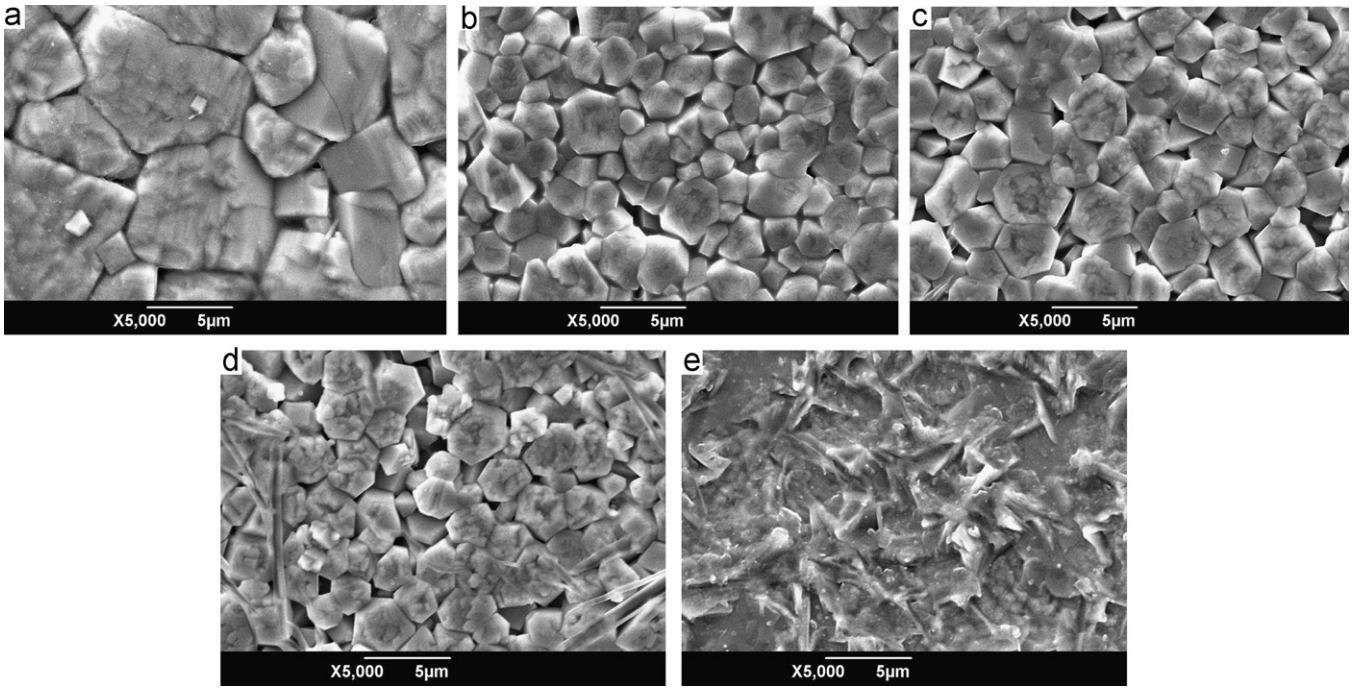

Fig. 5. Scanning electron micrographs for BSZT ceramics with different glass contents:(a) pure BSZT, (b) $x=5$, (c) $x=10$, (d) $x=15$ and (e) $x=20$.

The glass content dependence of BDS, grain boundary barrier $E_{a,1}$ and polar nanoregion trap energy $E_{a,2}$ for BSZT ceramics was illustrated in Fig. 7. The BDS value and grain boundary barrier $E_{a,1}$ increase gradually with enhance in glass content. While the trap energy $E_{a,2}$ nearly no changed with variation of glass content. Comparing the BDS curve with that of $E_{a,1}$, it is readily seen that a positive relationship presented between the BDS and the grain boundary barrier.

In fact, due to the presence of grain phases, glass phases and pores, ceramics usually performed as an inhomogeneous material. The distribution of electric field in material becomes vastly different under the external electric field. Considering the different electrical properties between grain boundary phases and grain phases, the double-layer dielectric model was employed to illustrate the distribution of electric field in this work. When a DC voltage was applied to the sample, both the electric field strengths corresponding to the two layers are different from the average electric field strength, which are given by

$$E_{gb} = \frac{\sigma_g(d_{gb}+d_g)}{\sigma_{gb}d_g+\sigma_g d_{gb}} \times E_{avg} \quad (2)$$

$$E_g = \frac{\sigma_{gb}(d_{gb}+d_g)}{\sigma_{gb}d_g+\sigma_g d_{gb}} \times E_{avg} \quad (3)$$

where E_{gb}, E_g, and E_{avg} are the electric field strength corresponding to grain boundary, grain and average value. σ_{gb} and σ_g are the electric conductivity corresponding to grain boundary and grain. d_{gb} and d_g are the thickness corresponding to grain boundary and grain, respectively. According to the complex impedance spectrum in Fig. 3, it can be deduced that the grain boundary resistance R_{gb} is far greater than the grain resistance R_g at room temperature, i.e. $\sigma_{gb} \ll \sigma_g$. Thus the grain boundary sustains higher electric field strength, which is more prone to result in breakdown than grain. Once the grain boundary layer was broken down, more voltage will apply to the grain layer, which leads to distorting of the electric field, and results in the grain layer is broken down as well. Consequently, the grain boundary plays a major role in determining the breakdown performance of ceramics.

In glass-added ferroelectric ceramics [12–14], the glass phase is usually located at grain boundaries and triple joints of particles, the grain size reduced notably with increasing glass content. However, the decrease of grain size results in a higher grain boundary density, i.e. more interfaces occurs between ferroelectric phase and glass. In addition, due to the big difference in dielectric constant between ferroelectric phase and glass, larger amounts of bulk charges will accumulate at the interfaces with increase in glass content. This leads to the obvious increase in the grain boundary barrier. On the other hand, it was observed [21] in materials with microstructures containing high interface densities, the dielectric BDS is improved when materials are able to stabilize a great amount of charges at room temperature. Higher grain boundary barrier limits the charge spreading behavior at the interfaces, which delays the breakdown performance, leads to the increase of E_b.

In order to investigate the energy storage properties, the P–E hysteresis loops for BSZT ceramics with different glass contents were measured at 1 Hz until the sample undergoes a breakdown and plotted in Fig. 8. It is worth noting that the polarization decreases gradually with increasing glass addition. It can be attributed to the glass phase diluting the BSZT phase.

The energy density charged (J_c), discharged (J_d) and energy efficiency (J_c/J_d) [22] as a function of glass content were calculated from the P–E hysteresis loops and presented in Fig. 9. The J_c and J_d increase first and then decrease gradually with increase in glass content. The addition of the glass improves the BDS of BSZT and consequently results in a higher energy density. Moreover, because of the low leakage currents, all samples possess a high energy efficiency of above 87.0%. Among all the measured samples, BSZT ceramic with 5 wt% glass addition has the highest J_d and J_c of 0.45 and 0.51 J/cm^3

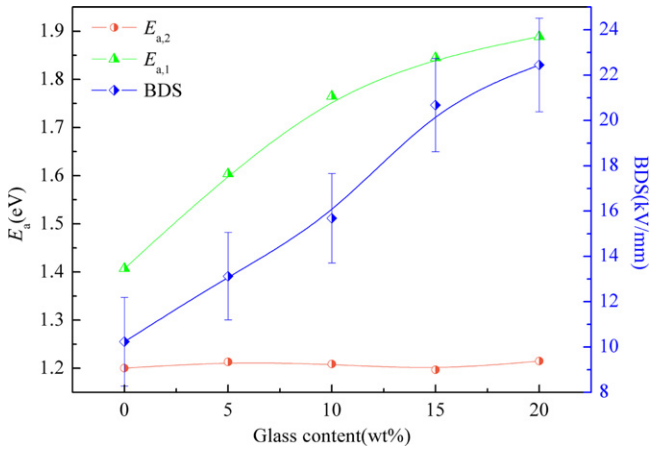

Fig. 7. Dielectric BDS and activation energy E_a as a function of glass content for BSZT ceramics.

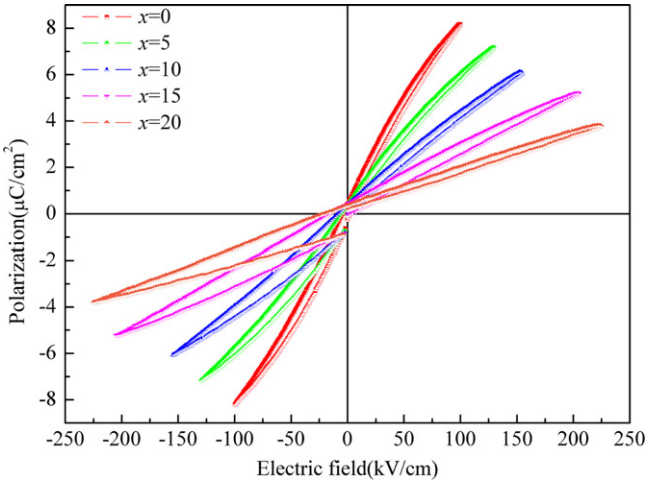

Fig. 8. P–E hysteresis loops for BSZT ceramics with different glass contents.

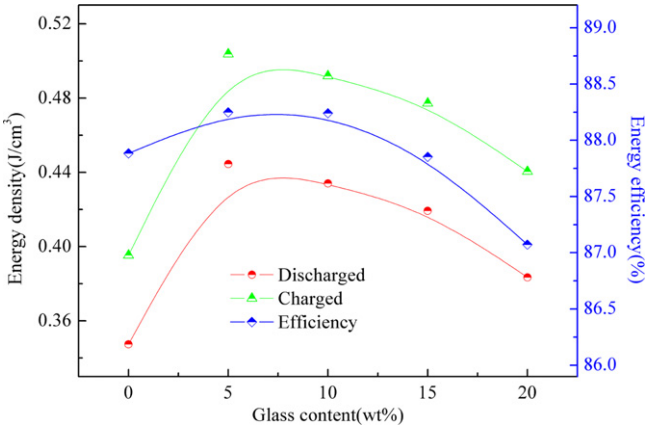

Fig. 9. Energy density and energy efficiency of BSZT ceramics as a function of glass content.

respectively, and which is accompanied by an energy efficiency of 88.2%.

4. Conclusion

$SrO–B_2O_3–SiO_2$ glass powders were prepared and employed as the sintering additives to reduce the sintering temperature of $Ba_{0.4}Sr_{0.6}Zr_{0.15}Ti_{0.85}O_3$ ceramics. The glass contents show a strong influence on the dielectric constant, microstructure, and discharged energy density. Impedance analysis suggests that there are two dielectric relaxation behaviors corresponding to the thermally activated motions of defect and polar nanoregions, respectively. The BDS result indicates that the ceramics have a more concentrative distribution of BDS with the increase in glass content. By comparing the glass content dependence of BDS and grain boundary barrier, it was found that the dielectric BDS of sample strongly depends on the grain boundary barrier. It can be concluded that it is the grain boundary barrier, by limiting the charge spreading behavior at the interfaces, which affects the breakdown performance of glass added ceramics. A discharged energy density of 0.45 J/cm^3 with an energy efficiency of 88.2% was achieved for $Ba_{0.4}Sr_{0.6}Zr_{0.15}Ti_{0.85}O_3$ ceramic with 5 wt% glass addition sintered at 1240 °C. These results provided useful information for barium strontium zirconate titanate in the application of energy storage capacitor ceramics.

Acknowledgments

This research was supported by the National Natural Science Foundation of China (51072106 and 51102159), the New Century Excellent Talents Program of Chinese Education Ministry (NCET-11-1042), the Foundation of Shaanxi Educational Committee (12JK0447), the International Science and Technology Cooperation Project Funding of Shaanxi Province (2012KW-06), the Academic Leaders Cultivation Program and the Graduate Innovation Fund of Shaanxi University of Science and Technology.

References

[1] A. Chakraborty, Advancements in power electronics and drives in interface with growing renewable energy resources, Renewable and Sustainable Energy Reviews 4 (2011) 1816–1827.
[2] M.S. Mirshekarloo, K. Yao, T. Sritharan, Large strain and high energy storage density in orthorhombic perovskite $(Pb_{0.97}La_{0.02})(Zr_{1-x-y}Sn_xTi_y)O_3$ antiferroelectric thin films, Applied Physics Letters 97 (2010) 142902.
[3] Y. Zhou, Q.M. Zhang, J. Luo, Q. Tang, J. Du, Structural and dielectric characterization of Gd_2O_3-added $BaO–Na_2O–Nb_2O_5–SiO_2$ glass–ceramic composites, Scripta Materialia 65 (2011) 296–299.
[4] B.J. Chu, X. Zhou, K.L. Ren, B. Neese, M.R. Lin, Q. Wang, F. Bauer, Q.M. Zhang, A dielectric polymer with high electric energy density and fast discharge speed, Science 313 (2006) 334–336.
[5] N.H. Fletcher, A.D. Hilton, B.W. Ricketts, Optimization of energy storage density in ceramic capacitors, Journal of Physics D: Applied Physics 29 (1996) 253–258.
[6] Y. Wang, B.Y. Liu, F. Wei, Z.M. Yang, J. Du, Effect of (Ba+Sr/Ti) ratio on the dielectric properties for highly (111) oriented (Ba, Sr)TiO_3 thin films, Journal of Alloys and Compounds 475 (2009) 827–831.
[7] Q.M. Zhang, L. Wang, J. Luo, Q. Tang, J. Du, $Ba_{0.4}Sr_{0.6}TiO_3$/MgO composites with enhanced energy storage density and low dielectric loss for solid-state pulse-forming line, International Journal of Applied Ceramic Technology 7 (2010) E124–128.
[8] C. Wang, B.L. Cheng, S.Y. Wang, H.B. Lu, Y.L. Zhou, Z.H. Chen, G.Z. Yang, Improved dielectric properties and tunability of multilayered thin films of $(Ba_{0.80}Sr_{0.20})(Ti_{1-x}Zr_x)O_3$ with compositionally graded layer, Applied Physics Letters 84 (2004) 5.
[9] S.B. Reddy, K.P. Rao, M.S.R Rao, Influence of A-site Gd doping on the microstructure and dielectric properties of $Ba(Zr_{0.1}Ti_{0.9})O_3$ ceramics, Journal of Alloys and Compounds 509 (2011) 1266–1270.
[10] Y.P. Shi, A.K. Soh, Effects of volume evolution of static and dynamic polar nanoregions on the dielectric behavior of relaxors, Applied Physics Letters 99 (2011) 092908.
[11] S. Singh, P. Singh, O. Parkash, D. Kumar, Structural and relaxor behavior of $(Ba_{1-x}La_x)(Ti_{0.85}Sn_{0.15})O_3$ ceramics obtained by solid state reaction, Journal of Alloys and Compounds 493 (2010) 522–528.
[12] Q.M. Zhang, L. Wang, J. Luo, Q. Tang, J. Du, Improved energy storage density in barium strontium titanate by addition of $BaO–SiO_2–B_2O_3$ glass, Journal of the American Ceramic Society 92 (2009) 1871–1873.
[13] A. Young, G. Hilmas, S.C. Zhang, R.W. Schwartz, Effect of liquid-phase sintering on the breakdown strength of barium titanate, Journal of the American Ceramic Society 90 (2007) 1504–1510.
[14] D. Zhang, T.W. Button, V.O. Sherman, A.K. Tagantsev, T. Price, D. Iddles, Effects of glass additions on the microstructure and dielectric properties of barium strontium titanate (BST) ceramics, Journal of the European Ceramic Society 30 (2010) 407–412.
[15] J.J. Huang, Y. Zhang, T. Ma, H.T. Li, L.W. Zhang, Correlation between dielectric breakdown strength and interface polarization in barium strontium titanate glass ceramics, Applied Physics Letters 96 (2010) 042902.
[16] N.G. Tyurnina, O.L. Belousova, A.I. Domanskii, L.A. Doronina, V.L. Ugolkov, Glass formation region and order of formation of crystalline phases in the $SrO–B_2O_3–SiO_2$ system, Glass Physics and Chemistry 36 (2010) 294–303.
[17] Z.J. Shen, W.P. Chen, J.Q. Qi, Y. Wang, H.L.W. Chan, Y. Chen, X.P. Jiang, Dielectric properties of barium titanate ceramics modified by SiO_2 and by $BaO–SiO_2$, Physica B 404 (2009) 2374–2376.
[18] D. Kumar, C.R. Gautam, O. Parkash, Preparation and dielectric characterization of ferroelectric $(Pb_xSr_{1-x})TiO_3$ glass ceramics doped with La_2O_3, Applied Physics Letters 89 (2006) 112908.
[19] M. Filippi, B. Kundys, R. Ranjith, A.K. Kundu, W. Prellier, Interfacial contribution to the dielectric response in semiconducting $LaBiMn_{4/3}Co_{2/3}O_6$, Applied Physics Letters 92 (2008) 212905.

[20] S.H. Yoon, C.A. Randall, K.H. Hur, Influence of grain size on impedance spectra and resistance degradation behavior in acceptor (Mg)-doped $BaTiO_3$ ceramics, Journal of the American Ceramic Society 92 (2009) 2944–2952.
[21] M. Touzin, D. Goeuriot, H.J. Fitting, C.G. Piecourt, D. Juve, D. Treheux, Relationships between dielectric breakdown resistance and charge transport in alumina materials—effects of the microstructure, Journal of the European Ceramic Society 27 (2007) 1193–1197.
[22] Y. Zhang, J.J. Huang, T. Ma, X.R. Wang, C.S. Deng, X.M. Dai, Sintering temperature dependence of energy-storage properties in (Ba, Sr)TiO_3 glass–ceramics, Journal of the American Ceramic Society 94 (2011) 1805–1810.